

Symmetry breaking in driven and strongly damped pendulum

Jukka Isohätälä,^{1,*} Kirill N. Alekseev,^{1,2,†} Lauri T. Kurki,¹ and Pekka Pietiläinen¹

¹*Department of Physical Sciences, P.O. Box 3000, University of Oulu FIN-90014, Finland*

²*Theory of Nonlinear Processes Laboratory, Kirensky Institute of Physics, Krasnoyarsk 660036, Russia*

(Dated: March 23, 2022)

We examine the conditions for appearance of symmetry breaking bifurcation in damped and periodically driven pendulum in the case of strong damping. We show that symmetry breaking, unlike other nonlinear phenomena, can exist at high dissipation. We prove that symmetry breaking phases exist between phases of symmetric normal and symmetric inverted oscillations. We find that symmetry broken solutions occupy a sufficiently smaller region of pendulum's parameter space in comparison to the statements made in earlier considerations [McDonald and Plischke, Phys. Rev. B 27 (1983) 201]. Our research on symmetry breaking in a strongly damped pendulum is relevant to an understanding of phenomena of dynamic symmetry breaking and rectification in a pure ac driven semiconductor superlattices.

PACS numbers: 05.45.-a, 02.30.Oz, 73.21.Cd, 74.50.+r, 72.20.Ht

Keywords: Pendulum; symmetry breaking; chaos; semiconductor superlattice; Josephson junction

I. INTRODUCTION

Periodically forced and damped pendulum

$$\ddot{\theta} + \gamma \dot{\theta} + \sin \theta = f \cos \omega t \quad (1)$$

is one of the most important paradigms in the modern nonlinear science [1]. In solid state physics, the pendulum model well describes, for instance, the nonlinear dynamics of Josephson junctions of superconducting materials [2, 3].

Fairly popular RSJ model of Josephson junction [4, 5], which is equivalent to an underdamped pendulum, $\gamma \ll 1$, demonstrates very rich nonlinear dynamics. Rotational states of the pendulum, $\langle \dot{\theta} \rangle \neq 0$ (averaging over a period $T = 2\pi/\omega$), correspond to a generation of dc voltage across the junction driven by ac current without dc component. Moreover, phase-locked states of the pendulum, $\langle \dot{\theta} \rangle = n/m$ (n and m are integers), correspond to quantized values of dc voltage in the Josephson junction model. This effect, known as the inverse ac Josephson effect [6, 7], has already found an application in the design of modern standard of one Volt [3, 8]. Chaotic vibrational and rotational motions of underdamped pendulum, $\gamma \ll 1$ are also well-known in Josephson junctions [9, 10] (for review see [11]). Surprisingly, the optimum operating point for the voltage standards in (ω, f) -parameter space is located near a region of chaos [3]. Therefore, knowledge of conditions for transition to chaos is important for the optimization of zero-bias voltage standard and related Josephson devices [3, 8].

One of the most often observable roads to chaos is the period doubling scenario [12]. The pendulum (1) belongs to a class of symmetric dynamical systems with the invariance under the transformations $\theta \rightarrow -\theta$ and

$t \rightarrow t + T/2$. Therefore, symmetry-breaking bifurcation is a necessary precursor to period doubling [10, 13, 14]. This bifurcation describes a sharp transition from a symmetric limit cycle satisfying

$$\theta(t + T/2) = -\theta(t) + 2\pi k \quad k \text{ is an integer} \quad (2)$$

to symmetry broken limit cycles, for which this equality is invalid. As easily seen from (1), a steady-state symmetric solutions, $\theta(t)$, can have only odd harmonics of ω in their Fourier expansion series, together with a zero harmonic $\langle \theta \rangle$ that is equal to either 0 or π . The solutions with $\langle \theta \rangle = 0$ are symmetric oscillations around the stable position $\theta = 0$, while $\langle \theta \rangle = \pi$ corresponds to oscillations of inverted pendulum. In contrast, for symmetry broken solutions both even and odd harmonics are possible and $\langle \theta \rangle$ is some constant different from 0 or π . Typically, the symmetry broken trajectories of underdamped pendulum occupy a very small range of parameters ωf just near transition to chaos [10, 13, 15]. Detailed analytical analysis of a transition from symmetric oscillations to symmetry broken oscillations near chaos border in the underdamped pendulum, $\gamma \ll 1$ and $\omega < 1$, is presented in [16].

In spite of a widely spread belief that symmetry breaking is always connected to a transition to chaos [14], this bifurcation is still possible for $\gamma \ll 1$ but $\omega > 1$ [17]. In these conditions chaos is impossible and symmetry breaking arises near transitions from normal to inverted states of the pendulum [17].

For a strong damping ($\gamma \gtrsim 1$), neither chaotic [18, 19], nor rotational phase locked states [10] can exist anymore. However, the presence of symmetry broken states of overdamped pendulum, that obviously are not related to a transition to chaos, has been briefly mentioned earlier in two papers devoted to dynamics of Josephson junctions [13, 20]. Moreover, it has been reported [13] that these symmetry broken trajectories occupy a quite large part of the parameter space (ω, f) . This interesting aspect of the pendulum dynamics at strong dissipation did not get

*Electronic address: jisojata@student.oulu.fi

†Electronic address: Kirill.Alekseev@oulu.fi

further attention so far, probably because of two main reasons. First, for the Josephson junctions pendulum's solutions at a strong damping are not physically interesting. Second, θ and $\langle\theta\rangle$ do not correspond to any directly measurable physical variables in the junctions.

However, it has been shown recently that another type of solid state microstructures – semiconductor superlattices subjected to a high-frequency electric field – can demonstrate very rich nonlinear dynamics similar to dynamics of the Josephson junctions [21, 22, 23, 24, 25, 26, 27]. In particular, an analog of inverse ac Josephson effect has been predicted for the superlattices [23, 25]. Moreover, within some reasonable approximations nonlinear dynamics of an ac-driven semiconductor superlattice in the miniband transport regime is governed by a periodically forced and damped pendulum [26, 27]. For the superlattices with realistic scattering constant [28, 29], an effective damping in the corresponding pendulum model is not small: $\gamma \gtrsim 1$. Overdamped pendulum also arises in the models of lateral semiconductor superlattices [30].

Importantly, in contrast to the case of Josephson junctions, a voltage across a superlattice is proportional to both the velocity, $\dot{\theta}$, and the coordinate, θ , of the pendulum (1) [26]. Therefore, even if rotations are impossible, $\langle\dot{\theta}\rangle \neq 0$, a dc voltage across the superlattice can still be generated due to contributions of symmetry-broken swinging oscillations with $\langle\theta\rangle \neq l\pi$ ($l = 0, 1$). For a strong damping, this is the only mechanism that can contribute to a rectification of THz signal in the semiconductor superlattice [26].

The existence of physical situations, where the symmetry breaking in pendulum at strong dissipation can be physically important, is the main motivation of our present work. Combining the analytical technique of truncated Fourier expansion [31] with numerical simulations we find the conditions for symmetry breaking at strong damping. We describe a scenario of transition from symmetric to asymmetric oscillations at a strong damping. We found that symmetry broken (SB) oscillations form an intermediate stage between symmetric normal (N) and symmetric inverted (I) oscillations, i.e. $N \rightarrow SB \rightarrow I \rightarrow SB \rightarrow N$. Note that it is different from transitions $N \rightarrow SB \rightarrow N$ with a large symmetry breaking phase even in overdamped case, which have been reported in [13]. We observed a relatively small symmetry breaking phase; with an increase of damping the ranges of driving amplitude and frequency, resulting in symmetry breaking, decreases. Moreover, symmetry breaking does not exist in the overdamped case described by the first order differential equation. In this case only normal and inverted oscillations survive. We presented simple formulas providing a good approximation for bifurcation points between different types of symmetric ($N \rightarrow I$) and asymmetric ($N \rightarrow SB$, $I \rightarrow SB$) transitions in wide ranges of the frequency and the strength of alternating force.

The organization of this paper is as follows. We start with a consideration of overdamped pendulum without inertial term ($\ddot{\theta} = 0$). The analysis of this model appears

to be the most simple and transparent. In the subsequent section III, we present analytic and numerical results on symmetry breaking bifurcations in the pendulum with inertial term. The final section of the paper is devoted to a summary and a brief discussion on applications in physics of semiconductors. The main text of our paper contains only most important results with sufficient explanations. Details of analysis and computing are presented in Appendixes: Analytic analysis of bifurcations in first- and second order pendulum equations (Appendix A), numerical methods in use (Appendix B), proof of absence of hysteresis at symmetry breaking transition (Appendix C) and role of higher order harmonics at symmetry breaking (Appendix D).

II. FIRST ORDER PENDULUM EQUATION

When damping is very strong we can neglect the second order derivative in (1) and get the first order overdamped pendulum equation

$$\dot{\theta} + \beta \sin \theta = \eta \cos \omega t \quad (3)$$

with $\beta = 1/\gamma$ and $\eta = f/\gamma$. Numerical integration of this equation shows that only two types of stable periodic motion exists: Normal and inverted modes of oscillations. Solutions corresponding to these modes are all symmetric with $\langle\theta\rangle = 0$ and $\langle\theta\rangle = \pi$ for the normal and inverted mode solutions, respectively. Figure 1 shows a plot of regions of the two different modes in the (f, ω) -parameter plane which exhibits a fan shaped pattern of alternating, disjoint areas of normal and inverted mode oscillations. A transition between the two modes is a sharp one and no intermittent states are in spite of rigorous attempts found. Especially, no symmetry broken regions exist.

A simple analytic calculation verifies the absence of symmetry broken solutions and provides a good approximate condition for the transition. The analysis is done under the assumption that the solution is well described by the trial function

$$\theta = A_0 + A_1 \cos(\omega t + \alpha_1). \quad (4)$$

We begin by applying linear stability analysis to find the regions of stable symmetric motion. For details refer to Appendix (A). Straightforward analysis leads to a stability condition

$$\beta \cos A_0 J_0(A_1) > 0, \quad (5)$$

where J_0 is the zeroth order Bessel function. If for the zeroth harmonic we have $\cos A_0 < 0$, then $J_0(A_1) > 0$ must apply and vice versa. Both symmetric solutions lose their stability at the same A_1 , which is a root of the Bessel function J_0 . As the Bessel functions and the zeros of J_0 will appear frequently, we adopt the shorthand notations

$$J_0(A^{(n)}) = 0, \quad J_k^{(n)} \equiv J_k(A^{(n)}), \quad (6)$$

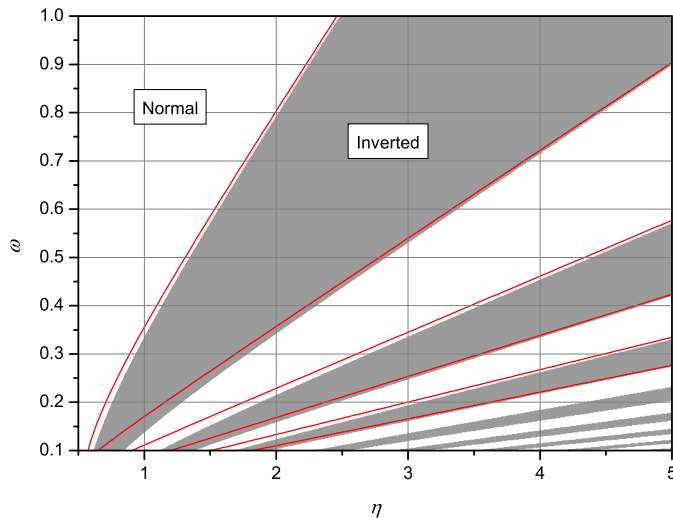


FIG. 1: (Color) First order pendulum, with $\beta = 1/2$, regions of inverted and normal mode oscillations. White areas correspond to normal oscillations with $\langle\theta\rangle = 0$ and gray areas to inverted mode, $\langle\theta\rangle = \pi$. No symmetry broken solutions are found. Solid (red) lines indicate the analytic prediction for mode boundaries, Eq. (8), which are plotted for $n = 1 \dots 6$.

where $A^{(n)}$ is specifically the n th root of J_0 and $J_k^{(n)}$ is J_k evaluated at $A^{(n)}$.

From the equation of motion, Eq. (3), we can derive using the ansatz (4) relation

$$J_0(A_1) \sin A_0 = 0. \quad (7)$$

From Eq. (7) it follows that if $A_0 \neq 0, \pi$, then $J_0(A_1) = 0$. However, stability condition (5) indicates that this case is not stable, as a perturbation does not decay. Therefore it is evident that asymmetric trajectories are not possible.

Within the applicability of our first order approximation, the only stable solutions are the ones with $A_0 = 0$ or π . Additionally, the pattern of normal and inverted mode solutions is revealed. Starting from a forcing η low enough, *i.e.* for which $J_0(A_1) > 0$, Eq. (5) implies that $A_0 = 0$. When A_1 crosses $A^{(1)}$, the sign must change in both factors, leading to $A_0 = \pi$. As η is further increased, A_1 reaches $A^{(2)}$ and the oscillations return to the normal mode.

The boundaries of the normal and inverted oscillations can even be written in an explicit analytic form. From Eq. (3) the expansion coefficient A_1 in (4) can be found as a function of pendulum parameters. Substituting $A_1 = A^{(n)}$ we get

$$4\beta^2 J_1^{(n)2} + \omega^2 A^{(n)2} = \eta^2. \quad (8)$$

Now we can compare our analytic results with numerical data. The boundaries of transitions between normal and inverted modes of oscillations, followed from Eq. (8), are

superimposed on the numerical results in Fig. 1. We see that the equality $J_0(A_1) = 0$ and the prediction of Eq. (8) hold well at the transition lines with reasonable accuracy everywhere, except in the case of low frequency. In the limiting case of very low frequency drive, the trial solution in the simplest form (4) can become invalid and effects of higher harmonics should be taken into account.

III. SYMMETRY BREAKING IN THE PENDULUM AT STRONG DISSIPATION

A. Numerical integration

Now we return to the pendulum with inertia, Eq. (1). We start with a review of our numerical results; for a detailed description of numerical methods see Appendix B. The study of (ω, f) -parameter plane reveals a fan shaped structure of regions of normal and inverted mode oscillations, similar to that of the first order pendulum. In addition to the alternating pattern of the symmetric solutions, narrow regions of symmetry broken solution have now emerged on the interfaces between the regions. For the solutions in these regions we have observed nonzero values of zero harmonic components along with nonzero even harmonics, which are requisites of a symmetry-broken solution. The different modes on the parameter plane are depicted in Fig. 2, where we have chosen $\gamma = 2$ for the damping coefficient. Symmetry broken regions appear around both transitions, from normal to inverted and back, thus separating the normal and inverted mode

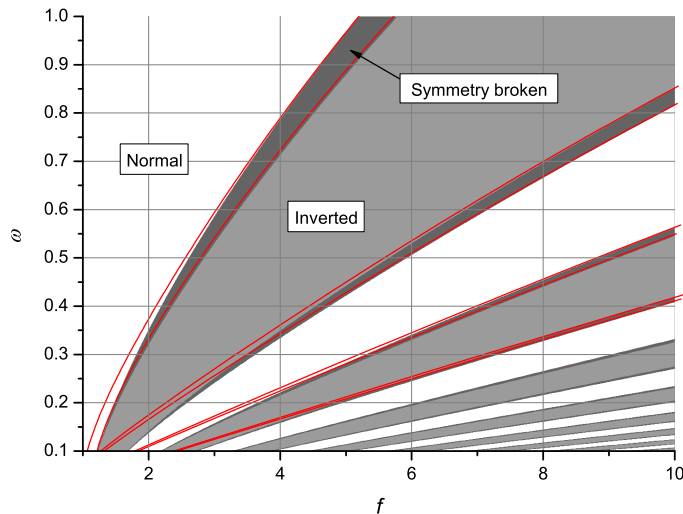


FIG. 2: (Color) Second order pendulum equation, regions of inverted and normal state oscillations. Sandwiched between them are the regions of symmetry breaking. Solid (red) lines indicate analytic prediction of Eqs. (12) and (10).

regions completely. Regions are not wide, in contrast to what was reported in [13] [41]. Increasing the damping will cause them to get more narrow. A closer examination is shown in Fig. 3, where we have fixed $\omega = 0.2$ and $\gamma = 3$. Harmonic components A_0 and A_1 are plotted against the drive amplitude f , and the sequence of modes of solutions is made more clear. Normal mode bifurcates into asymmetric solutions when A_1 is close to a root of the Bessel function $J_0(A_1)$. This symmetry broken state persists only for a short interval of variable f , ending in inverted mode, when A_0 has reached π . Small deviations from approximately linear response of A_1 to a change of f can be seen at the transitions from normal to inverted mode.

Close-ups of the symmetry-broken range provide more insight. The following two examples are depicted in Fig. 4. The first case we consider is of low frequency drive, $\omega = 0.2$ and $\gamma = 3$. Symmetry breaking starts for moderate forcing, $f = 1.8413$ and with A_1 slightly larger than $A^{(1)}$, the first root of J_0 . The curve of A_0 of stable symmetric solution bifurcates from zero into a curve corresponding to a stable asymmetric solution. This is accompanied with the emergence of even harmonics in the Fourier spectrum and a sudden stop in the increase of A_1 . Further increases of f cause A_1 to decrease, while A_2 traces a sugar-loaf shaped curve. It should be noted, that the curve of the second harmonic reaches quite high values, $A_2 \sim 0.6$ at the maximum. The zero harmonic varies continuously and monotonously from zero to π . We should note that actually two different stable solutions exist in the symmetry breaking range, that are related to each other by the symmetry. Initial values of the

system determine which branch the solution converges to after the initial transient. Symmetry breaking ends in an inverted state at $f = 1.8773$ with A_1 just less than $A^{(1)}$.

In the second case we examine, we set $\omega = 4$ and $\gamma = 3$. To achieve symmetry breaking, one needs high values of f . In this case we have $f = 47.46$. Again, A_1 has just crossed $A^{(1)}$ when the symmetric mode loses stability. Now the decrease of A_1 in the symmetry broken region is less dramatic than in the low frequency case. Furthermore, the second harmonic component is almost negligible. In other respects, this case doesn't differ from the previous example.

B. Analytic analysis

In this subsection we present explicit analytic form of conditions for the bifurcation to occur and provide a picture of the scenario of symmetry breaking that is consistent with the numerical results. Here, as in Sec. II, we assume that oscillations of the pendulum can be described by the trial function in the form (4). For details and discussion on the range of validity of our analytic results, see Appendix A.

Following the method of [10, 31], we linearize Eq. (1) and, with appropriate approximations, put it into the form of the Mathieu equation. Using the existing knowledge of the solutions of Mathieu equation, we derive the following conditions for bifurcations from symmetric oscillations

$$J_0(A_1) + (-1)^k \frac{2}{\gamma^2 + 4\omega^2} J_2(A_1)^2 = 0, \quad (9)$$

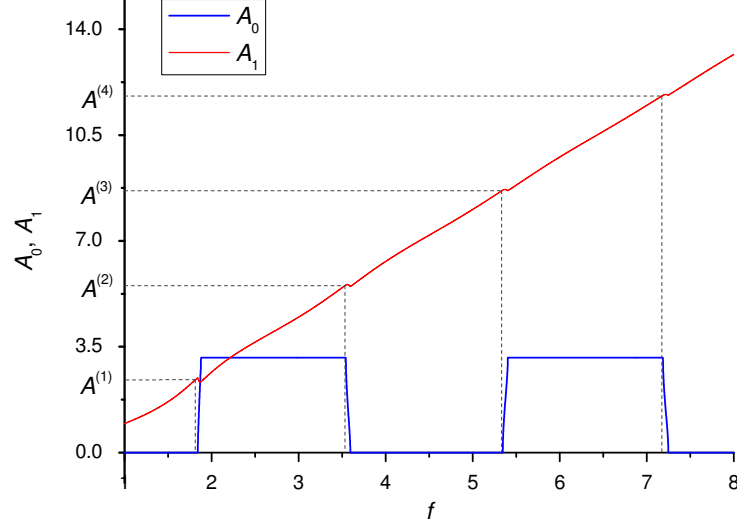


FIG. 3: (Color) The amplitudes of the two first harmonic components, A_0 (blue) and A_1 (red) plotted against f . A_1 shows nearly linear dependence on parameter f . Small deviations from this are seen near the transitions between normal and inverted states, along with a A_0 component that is not equal to 0, π . To guide the eye, dashed lines connecting the points $A_1(f) = A^{(n)}$ on the vertical axis to the corresponding f on the horizontal axis are drawn. The fixed pendulum parameters are $\gamma = 3$ and $\omega = 0.2$.

where $k = 0$ corresponds to a normal mode, while $k = 1$ marks an inverted mode. Notice, that Eq. (9) is the same condition for loss of stability as the one for the first order pendulum, $J_0(A_1) = 0$, but now with an additional term. This term only becomes significant when A_1 is close to a root of the Bessel function J_0 . As a consequence, now there are two separate bifurcation points corresponding to the two different symmetric modes. These are located rather close to the roots of J_0 . Clearly, the dynamics of the second and the first order pendula are similar away from the regions of transition, justifying the correspondence to the analysis of the previous section.

The explicit solution of Eq. (9) in terms of amplitude A_1 can now be found. Owing to the fact that the latter term in Eq. (9) is small, we get for the critical values of A_1

$$\left. \begin{aligned} A_N^{(n)} \\ A_I^{(n)} \end{aligned} \right\} = A^{(n)} \pm \frac{2J_2^{(n)2}}{J_1^{(n)}(\gamma^2 + 4\omega^2) \mp \chi^{(n)}}, \quad (10)$$

$$\chi^{(n)} = 2J_2^{(n)}(J_1^{(n)} - J_3^{(n)}). \quad (11)$$

Here $A_N^{(n)}$ and $A_I^{(n)}$ are respectively the critical amplitudes of normal and inverted modes for which symmetric oscillations become unstable. A small asymmetry with respect to $A^{(n)}$ in the critical A_1 due to the term $\chi^{(n)}$ can be neglected within the applicability of Eq. (10) without loss of qualitative agreement. This is implicitly assumed hereafter in this section.

In transitions from normal to the next inverted mode, critical value of amplitude A_1 for the inverted mode is

less than that of the normal mode: $A_I^{(n)} < A_N^{(n)}$. The reverse applies for transitions from an inverted phase to the next normal phase region, *i.e.* $A_N^{(n)} < A_I^{(n)}$. Therefore A_1 must decrease as the boundary of the first symmetry broken region is crossed, and the n th region starts when $A_1 > A^{(n)}$ and ends when $A_1 < A^{(n)}$. Such kind of behavior of A_1 is in a good agreement with numerical results shown in Fig. 4. Moreover, following Eq. (10) the difference between $A_N^{(n)}$ and $A_I^{(n)}$ decreases with an increase of the frequency ω . This explains why the range of A_1 within the symmetry breaking region is wider in the low frequency case in comparison with the case of high frequency drive (cf subplots (a) and (b) in Fig. 4).

We turn now to finding of surfaces in the parameter space (γ, ω, f) , on which the symmetry breaking bifurcation happens. First, we substitute the trial solution (4) in the equation of motion (1) and in the first harmonic approximation derive the dependence of amplitude A_1 on the pendulum parameters γ , ω and f . Second, substituting critical values of A_1 from Eq. (10) and taking $A_0 = k\pi$, we have

$$f^2 = (\gamma\omega A_1)^2 + (\omega^2 A_1 \pm 2J_1(A_1))^2, \quad \begin{cases} A_1 = A_I^{(n)} \\ A_1 = A_N^{(n)} \end{cases} \quad (12)$$

for bifurcations from inverted and normal modes, respectively. Taking the difference of these two critical f does indicate that one symmetric mode loses stability before the other gains it. This eliminates a possibility of hysteresis around the symmetry breaking transition and shows that both symmetric phases cannot be stable for same

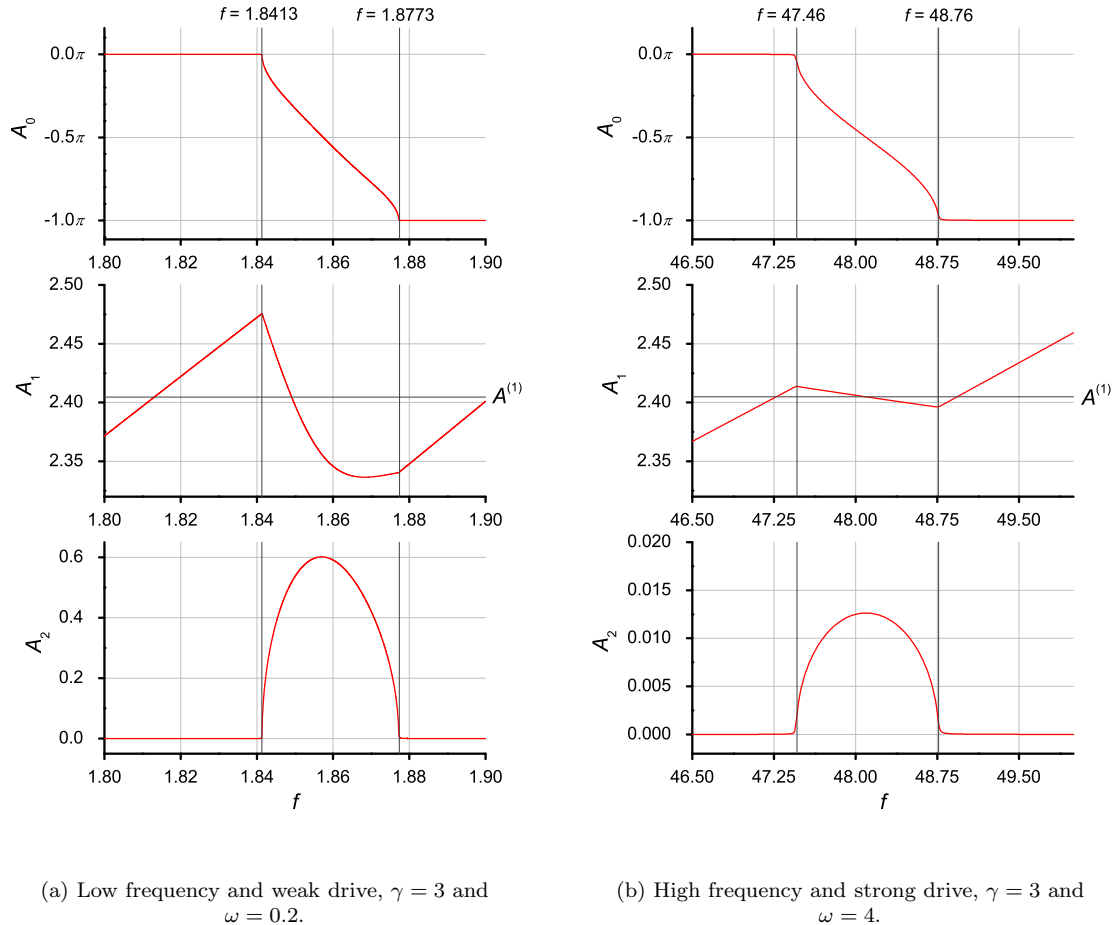


FIG. 4: (Color) The amplitudes of the two first harmonic components as functions of the drive amplitude f . Notice the relatively large amplitude of the second harmonic component in the low frequency case.

pendulum parameters. For more detailed discussion on this subject, see Appendix C.

Our main analytic results, Eqs. (12) and (10), are expected to be valid for $\omega \gtrsim 1$. Even for frequencies less than unity, these results may be applied, provided that f is sufficiently large. Increasing the damping does somewhat improve results, and for low frequency overdamped case, good qualitative picture can be still provided even for low frequencies, $\omega \simeq 0.1$ (see Appendix A). The effects of third and higher order harmonics in the trial solution (4) are discussed in Appendix D.

On the other hand, Eq. (12) shows remarkable agreement with the numerical results for a very wide range of parameters. In Fig. 2 analytic prediction for the boundaries of symmetry breaking regions are shown as solid (red) lines. Additionally, in Table I we have tabulated points of symmetry breaking bifurcations in f variable for a selected set of quite different values of ω and γ . Boundaries of regions of stable symmetric solutions can be found even in low damping and moderately low frequency case, provided that f is sufficiently large. This

suggests that as damping or frequency are lowered from sufficiently high values, the symmetry broken regions evolve into the regions of complex and chaotic dynamics with the alternating normal and inverted phase motion separating them. Evidently, our analytic results provide a reasonable approximation even in parameter space regimes beyond only overdamped case.

Now we can summarize the main results of present section. Taking the alternating force strength, f , as the control parameter, we can report the following behavior: A stable inverted or normal mode becomes unstable at an amplitude of stationary oscillations, A_1 , that is just greater than $A^{(n)}$ and symmetry breaking starts. Increasing f further causes A_1 to decrease, as the bifurcation to the next mode should occur when A_1 is less than $A^{(n)}$. The critical values of the A_1 are given by Eq. (10) with the critical parameters by Eq. (12). These critical points approach a common value, $A^{(n)}$, as damping is increased.

Parameters			Numerical		Analytic		Errors (%)	
γ	ω	n	f_1	f_2	f_1	f_2	e_{Max}	e_{Width}
2	1	1	5.19964	5.76731	5.22416	5.7492	0.48	7.6
3	2	2	39.4625	40.1666	39.4589	40.1622	0.011	0.11
0.05	2	1	8.76666	10.51386	8.79088	10.5046	0.28	2.0
0.5	1	2	5.61680	6.79113	5.60002	6.76786	0.35	0.56
0.5	0.5	3	2.73651	3.53534	2.71429	3.45881	2.2	6.8

^aRegion between the critical f involves in addition to symmetry broken solutions also complex dynamics including chaos.

TABLE I: Locations and widths of selected symmetry breaking intervals. Here (γ, ω, n) are the parameters of the system with n being the number of the transition. The start and end points of the symmetry broken range are, respectively, f_1 and f_2 . In the errors' column, e_{Max} is the larger of the relative errors in the start or end points of the symmetry breaking interval. Additionally the error in the width of the symmetry broken interval e_{Width} is given. Analytically given values for the start and end points are obtained using Eq. (12) along with Eq. (10). Notice the good agreement between the analytic and numerical result even for very low damping and moderate frequencies.

IV. CONCLUSION

In summary, we confirmed the existence of symmetry breaking phenomenon in the strongly damped pendulum. The symmetry breaking states form a necessary stage in transitions from the normal to the inverted and from the inverted to the normal states of the overdamped pendulum. The scenario of transitions from the symmetric to the symmetry broken states, and vice versa, appears to be similar to the case of underdamped pendulum without chaos [17]. Our results also demonstrate that an inertial term in pendulum is a requisite of symmetry breaking. On a more hypothetical note, it could then be possible to achieve symmetry breaking similar to what it described here, if higher even derivatives or/and additional nonlinear damping terms are included.

These results can be directly applied to the studies of novel mechanism of THz radiation rectification in semiconductor superlattices [25] because this system has underlying pendulum dynamics [26, 30]. Note that in some cases pendulum-like equation of the third order [32, 33] and a pendulum equation with a nonlinear damping term supporting symmetry of the problem [34] naturally arise in different models of semiconductor superlattices. We speculate that swinging symmetry broken oscillations in these superlattice models also correspond to a spontaneous generation of dc voltage or dc current. Related detailed consideration will be published elsewhere. It is worth to notice also the importance of the symmetry breaking bifurcations in the physics of ac-driven bulk semiconductors with different types of nonlinearity [35]. Our results can be also useful in the development of this area of semiconductor nonlinear dynamics.

Acknowledgments

This research was partially supported by the Academy of Finland, grants No 1206063 and No 100487.

APPENDIX A: DETAILS OF ANALYTIC ANALYSIS

1. First order pendulum

We start with a derivation of stability condition (5). Consider a small perturbation $\delta(t)$ to a solution of Eq.(3). The evolution of the perturbation is governed by the linearized equation

$$\dot{\delta} + \beta \cos \theta \delta = 0. \quad (\text{A1})$$

Its formal solution is

$$\delta = \exp \left(-\beta \int dt \cos \theta \right). \quad (\text{A2})$$

Using Eq. (4) and well known identities

$$\sin(a \cos \phi) = 2 \sum_{n=0}^{\infty} (-1)^n J_{2n+1}(a) \cos((2n+1)\phi), \quad (\text{A3})$$

$$\cos(a \cos \phi) = J_0(a) + 2 \sum_{n=1}^{\infty} (-1)^n J_{2n}(a) \cos(2n\phi), \quad (\text{A4})$$

the solution $\delta(t)$ is put into the form

$$\delta = \exp(-\beta \cos A_0 J_0(A_1)t + \text{periodic terms}). \quad (\text{A5})$$

A perturbation to a stable solution must be damped, which leads to the stability condition (5).

Now we turn to the derivation of Eq. (8). We substitute the ansatz into Eq. (3). Identities (A3) and (A4), truncated to include terms up to the first harmonic, are now employed to expand the sine term. Finally, in the resulting expression equating the trigonometric functions separately along with the zero harmonic, the following set of equations is obtained.

$$-2\beta \cos A_0 J_1(A_1) = \eta \cos \alpha_1 \quad (\text{A6a})$$

$$\omega A_1 = \eta \sin \alpha_1 \quad (\text{A6b})$$

$$J_0(A_1) \sin A_0 = 0 \quad (\text{A6c})$$

Eliminating the phase between Eqs. (A6a) and (A6b) we get

$$4\beta^2 \cos^2 A_0 J_1(A_1)^2 + \omega^2 A_1^2 = \eta^2. \quad (\text{A7})$$

Eq. (8) follows by substituting $A_1 = A^{(n)}$ and $A_0 = 0, \pi$.

2. Second order pendulum

a. Derivation of Eqs. (9) and (10)

Linearization of Eq. (1) yields the equation for the evolution of an infinitesimal perturbation

$$\ddot{\delta} + \gamma \dot{\delta} + \cos \theta \delta = 0. \quad (\text{A8})$$

Change of variables $\delta = \exp(-\gamma t/2) \xi$ removes the first order derivative term. The trial function (4) is again used to substitute θ and the cosine is expanded up to second order, as the first order term vanishes for symmetric mode solutions. Finally, after rescaling the time $\tau = \omega t + \alpha_1$, Eq. (A8) is put into the form

$$\ddot{\xi} + \frac{(-1)^k}{\omega^2} \left[J_0(A_1) - (-1)^k \frac{\gamma^2}{4} - 2J_2(A_1) \cos 2\tau \right] \xi = 0. \quad (\text{A9})$$

Overdot stands for differentiation with respect to τ and we use $A_0 = k\pi$. It is easy to see that Eq. (A9) has the form of the Mathieu equation,

$$\ddot{y} + (a - 2q \cos 2\tau)y = 0, \quad (\text{A10})$$

when we make the identifications

$$a = \frac{(-1)^k 4J_0(A_1) - \gamma^2}{4\omega^2}, \quad (\text{A11})$$

$$q = \frac{(-1)^k}{\omega^2} J_2(A_1). \quad (\text{A12})$$

Following Floquet theorem, a solution of Mathieu equation can be presented in the form $y = P(\tau) \exp(i\nu\tau)$, where P is a periodic function and ν is the Mathieu characteristic exponent. Stability of the symmetric oscillations is now determined by the condition

$$-\frac{\gamma}{2\omega} - \Im m \nu < 0, \quad (\text{A13})$$

which holds for stable solutions. Therefore, a symmetric solution loses stability at $\nu = -i\gamma/2\omega$. Real part of ν is zero.

We now turn to finding the points of bifurcation. We can make use of the expression for a as a function of q and ν [36] as

$$a = \nu^2 + \frac{q^2}{2(\nu^2 - 1)} + \dots, \quad (\text{A14})$$

which we truncate to include only the two first terms. Substituting the expressions for ν , a and q into (A14), we

obtain Eq. (9), which is the condition for a bifurcation from a symmetric solution. Note that the truncation of series (A14) is valid provided that q is small or ν^2 is large. These conditions are usually satisfied, independent of ω , because higher order terms are all proportional to $1/\omega^2$. Large damping is then needed for small ω in order to have the series converge fast enough for the truncation to apply.

Equation (9) can be approximately solved. We substitute $A_1 = A^{(n)} + \varepsilon$ and make a series expansion up to the first order in ε .

$$2(-1)^k J_2^{(n)^2} + \varepsilon \left[-(\gamma^2 + 4\omega^2) J_1^{(n)} + (-1)^k \chi^{(n)} \right] = 0, \quad (\text{A15})$$

where $\chi^{(n)}$ is defined in Eq. (11). The validity of this approach is due to the fact that the second term in Eq. (9) is small for wide range of parameters. It is obvious that $\gamma^2 + \omega^2 \gg 1$ is sufficient. However, this can be even slightly relaxed. Symmetry breaking is expected when A_1 is near a root of J_0 . Now, due to known properties of Bessel functions, we may infer that if A_1 is sufficiently large and near a root of J_0 , it is also close to a root of J_2 . Thus, the discussed second term may be small even for low values of γ and ω .

Resulting equation (A15) is trivial to solve for ε . Solution yields

$$\varepsilon = \frac{2(-1)^k J_2^{(n)^2}}{J_1^{(n)}(\gamma^2 + 4\omega^2) - (-1)^k \chi^{(n)}}, \quad (\text{A16})$$

from which Eq. (10) immediately follows. Note that the $\chi^{(n)}$ in the denominator results in a slight asymmetry of the bifurcation points with respect to $A^{(n)}$. Within the applicability of our results, $\chi^{(n)}$ is small enough to be neglected, when a more tractable form of Eq. (A16) is needed. Some of the quantitative agreement is lost in this approximation, but qualitative the result is the same. This is due to the fact that in the derivation of Eq. (A15) we already assumed, that $\gamma^2 + \omega^2$ is sufficiently large, or that $J_2(A_1)$ is small.

b. Derivation of Eq. (12)

Substituting the trial solution $\theta = A_0 + A_1 \cos(\omega t + \alpha_1)$ into the Eq. (1), expanding the $\sin \theta$ term using the second order truncations of identities (A4) and (A3) and finally equating the harmonic terms, the following set of equations is obtained

$$\sin A_0 J_0(A_1) = 0, \quad (\text{A17a})$$

$$2 \cos A_0 J_1(A_1) - \omega^2 A_1 = f \cos \alpha_1, \quad (\text{A17b})$$

$$-\gamma \omega A_1 = f \sin \alpha_1. \quad (\text{A17c})$$

Eliminating phase between Eqs. (A17b) and (A17c) we get

$$f^2 = (\gamma \omega A_1)^2 + (\omega^2 A_1 - 2 \cos A_0 J_1(A_1))^2. \quad (\text{A18})$$

Replacing A_0 and A_1 with values corresponding to the bifurcations of normal and inverted modes, we end up with an explicit expression for critical points, Eq. (12).

APPENDIX B: ON NUMERICAL METHODS

In all numerical calculations, standard double precision floating point arithmetic has been used. For the numerical integration of system (1), the equation is put into the form

$$\begin{aligned}\dot{\theta}_1 &= \theta_2, \\ \dot{\theta}_2 &= -\gamma\theta_2 - \sin\theta_1 + f\cos\omega t,\end{aligned}\quad (\text{B1})$$

where $\theta_1 \equiv \theta$. Initial values $\theta_k(0) = 0$, $k = 1, 2$, were used in all computations. The 4/5th order embedded Runge-Kutta routine with Cash-Karp coefficients [37] is used in majority of computations in this paper. For the comparison of analytic and numerical results on the symmetry breaking regions, Table I, 7/8th order Runge-Kutta with Prince-Dormand coefficients [38] was employed. In variable step-size control, a relative accuracy of around 10^{-10} was typically used.

Harmonic components were extracted from the numerical solution by introducing additional differential equations of the form

$$\dot{\xi}_0 = \theta, \quad \dot{\xi}_k = \theta \cos k\omega t, \quad \dot{\zeta}_k = \theta \sin k\omega t, \quad (\text{B2})$$

for $k > 0$. Same error bounds and step functions were used as for the variables θ_1 and θ_2 . Coefficients in the Fourier series expansion

$$\theta = a_0 + \sum_{k=1}^{\infty} (a_k \cos k\omega t + b_k \sin k\omega t) \quad (\text{B3})$$

have been evaluated using

$$a_0 = \frac{1}{T} (\xi_0(t_0 + T) - \xi_0(t_0)), \quad (\text{B4})$$

$$a_k = \frac{2}{T} (\xi_k(t_0 + T) - \xi_k(t_0)), \quad (\text{B5})$$

$$b_k = \frac{2}{T} (\zeta_k(t_0 + T) - \zeta_k(t_0)). \quad (\text{B6})$$

This simply amounts to calculating the projection of the solution onto orthogonal base of trigonometric functions. Finally, cosine harmonic coefficients of the series

$$\theta = A_0 + \sum_{k=1}^{\infty} A_k \cos(k\omega t + \alpha_k), \quad (\text{B7})$$

are computed using

$$A_k = \sqrt{a_k^2 + b_k^2} \quad (\text{B8})$$

$$-\alpha_k = \begin{cases} \arctan\left(\frac{b_k}{a_k}\right), & a_k > 0 \\ \arctan\left(\frac{b_k}{a_k}\right) - \pi, & a_k < 0 \\ \frac{b_k}{|b_k|} \frac{\pi}{2}, & a_k = 0 \end{cases} \quad (\text{B9})$$

Initial transient phase was eliminated by first performing a period search on the solution. A simple integration in steps of one drive cycle, $T = 2\pi/\omega$, was made and after each step the current values of θ and $\dot{\theta}$ were recorded and compared against the values of previous steps. A period of nT is assumed, if

$$|\theta_k(t) - \theta_k(t - nT)| < \epsilon (|\theta_k(t)| + |\theta_k(t - nT)|),$$

applies for $k = 1, 2$ (or just $k = 1$ for the first order pendulum). Tolerance is determined by the parameter ϵ . Typically, a value of $\epsilon = 10^{-9}$ was used. When near bifurcation points, lower values were needed, $\epsilon = 10^{-11}$ with correspondingly higher integrator accuracy requirements.

To determine numerically the bifurcation points reported in Table I, a finite time maximal Lyapunov exponent was used [39, 40]. Because one requires possibly a very long integration time to reach the stable limit cycle in the vicinity of bifurcation points, it was not deemed feasible to find the actual values of the harmonic components. Rather, Lyapunov exponent as a measure of the rate of convergence of a small perturbation is good indicator of bifurcation points, as it tends to zero as the critical point is approached.

APPENDIX C: ABSENCE OF HYSTERESIS

In Section IIIB it was stated that there is no hysteresis around symmetry breaking transition, because one symmetric mode loses stability before another gains it. However, actually situation is more complicated because regions of stability of symmetric normal and inverted modes do overlap, if one considers just A_1 as the variable. In this Appendix we will show that there is no contradiction between overlapping of regions of stability of the symmetric modes in (A_0, A_1) -plane and absence of such overlapping in (f, ω) -plane.

To begin with we want to demonstrate that the stability regions in units A_1 really can overlap. If the asymmetry of the bifurcation points with respect to $A^{(n)}$ in Eq. (A16) is neglected, the critical values of A_1 for stability are given by

$$\left. \begin{matrix} A_N^{(n)} \\ A_I^{(n)} \end{matrix} \right\} = A^{(n)} \pm \varepsilon_A \quad (\text{C1})$$

$$\varepsilon_A = \frac{2}{\gamma^2 + 4\omega^2} \frac{J_2^{(n)^2}}{J_1^{(n)}}. \quad (\text{C2})$$

Clearly, $\varepsilon_A < 0$ for even and $\varepsilon_A > 0$ for odd n . As odd n correspond to transitions from normal to inverted mode (N→I) and the other way around (I→N) for even n , the stability regions overlap.

Now we consider the difference between critical points of stability in variable f . We substitute (C1) in (A18) and expand in ε_A up to first order, then substitute k and A_1 with values corresponding to inverted and normal modes. Taking the difference of these values gives

$$\Delta f^2 \equiv f_1^{(n)^2} - f_N^{(n)^2} \quad (C3)$$

$$\approx -4\varepsilon_A A^{(n)} \omega^2 (\gamma^2 + \omega^2) + 8J_1^{(n)} \omega^2 A^{(n)} + 8J_1^{(n)} J_2^{(n)} \varepsilon_A. \quad (C4)$$

We next drop the last term, as it is small under the assumptions we have made earlier in derivation of Eq. (C1). Overlapping can occur when Δf^2 is negative for $n = 1, 3, \dots$ and when Δf^2 is positive for $n = 2, 4, \dots$. For n being odd this condition results in

$$\frac{\gamma^2 + \omega^2}{\gamma^2 + 4\omega^2} J_2^{(n)^2} > J_1^{(n)^2}, \quad (C5)$$

which holds if regions of stability overlap. Estimating left

hand side upwards, $(\gamma^2 + \omega^2)/(\gamma^2 + 4\omega^2) < 1$, we have $J_2^{(n)^2} > J_1^{(n)^2}$, which is false. Analogously the case of even values of n can be considered. These considerations confirm that both symmetric modes cannot be stable simultaneously for same values of parameter f .

APPENDIX D: APPLICABILITY OF THE FIRST HARMONIC TRIAL FUNCTION

The analytic results derived herein all rely upon the assumption that $\theta = A_0 + A_1 \cos(\omega t + \alpha_1)$ is a good approximation of a correct T -periodic solution or at least captures the essential features of it. Numerical integration of systems (1) and (3) indicate that at least when $\omega \gtrsim 1$ applies the higher harmonic components are insignificant. For analytic analysis we included the third harmonic term into the trial function, $\theta = k\pi + A_1 \cos(\omega t + \alpha_1) + A_3 \cos(3\omega t + \alpha_3)$. Substituting it in motion equation (1) we get

$$A_3 = \frac{6(-1)^k \omega^2 J_0(A_1) J_1(A_3) + (-1)^l 2\omega \sqrt{-\gamma^2 J_0(A_1)^2 J_1(A_3)^2 + (\gamma^2 + 9\omega^2) J_0(A_3)^2 J_3(A_1)^2}}{3\omega^2 (\gamma^2 + 9\omega^2)}, \quad (D1)$$

where l is an integer determined by conditions not essential to current analysis. Eq. (D1) vanishes as $1/\omega^2$ for high frequencies, in support of the numerical result. It is noteworthy that A_1 , and consequently f , are coupled to A_3 only via the Bessel functions in the numerator. Thus, high values of f and A_1 cannot increase significantly the third harmonic. Strong external drive therefore makes the relative contribution of the higher harmonics smaller. Clearly, problems can arise when the frequency is very low. Numerical integration also shows, that higher harmonics become more significant and even Eq. (D1) breaks down. Although individual harmonic components may have relatively low values, we have observed that the spectrum as a whole can be quite spread. Therefore, in this limiting case an inclusion of the first two or three harmonics into the trial function may not be enough.

Now we discuss the influence of damping. Surprisingly, we have found that in general an increase of damping does not always suppress the higher harmonics. From Eq. (D1) we have

$$A_3 \propto \frac{1}{\omega \gamma} \sqrt{J_0(A_3)^2 J_3(A_1)^2 - J_0(A_1)^2 J_1(A_3)^2} \quad (D2)$$

for very large damping. A_3 can be large even for large γ , if frequency is low. The Bessel functions become significant and strongly nonlinear response to an increase of γ is expected. Numerical integration confirms this. Relative amplitude of the third harmonic with respect to A_1 fluctuates with an increasing amplitude as γ is increased. Eventually these fluctuation will die out. There is an upper limit for γ , approximately given by (12) when $n = 1$, for which a symmetry breaking bifurcation can happen. We have observed numerically that after this final critical γ is crossed, fluctuation stop and the higher harmonics slowly fade away.

In summary, the first harmonic approximation of the solution is definitely valid when $\omega \gtrsim 1$. Increasing damping alone will not make the truncation more applicable in the regime, where interesting phenomena are expected. It will improve the accuracy of some results presented in this paper, which rely on assumption that $\omega^2 + \gamma^2$ is large. Specifically, overdamped case is well described even for $\omega \sim 0.1$, albeit without impressive quantitative agreement. High values of parameter f result in higher relative proportion of the first harmonic component in the solution, thus improving the approximation.

[1] R. Z. Sagdeev, D. A. Usikov, and G. M. Zaslavsky, *Nonlinear Physics: From the Pendulum to Turbulence and*

Chaos (Harwood Academic Publishers, Chur, Switzerland, 1992).

- [2] K. Likharev, *Dynamics of Josephson junctions and circuits* (Gordon and Breach, New York, 1986).
- [3] R. L. Kautz, Rep. Prog. Phys. **59**, 935 (1996).
- [4] D. E. McCumber, J. Appl. Phys. **39**, 3113 (1968).
- [5] W. C. Stewart, Appl. Phys. Lett. **12**, 277 (1968).
- [6] D. N. Langenberg, D. J. Scalapino, B. N. Taylor, and R. E. Eck, Phys. Lett. **20**, 563 (1966).
- [7] M. T. Levinsen, R. Y. Chiao, M. J. Feldman, and B. A. Tucker, Appl. Phys. Lett. **31**, 776 (1977).
- [8] C. A. Hamilton, Rev. Sci. Instr. **71**, 3611 (2000).
- [9] B. A. Huberman, J. P. Crutchfield, and N. H. Packard, Appl. Phys. Lett. **37**, 750 (1980).
- [10] D. D’Humieres, M. R. Beasley, B. A. Huberman, and A. Libchaber, Phys. Rev. A **26**, 3483 (1982).
- [11] U. Krüger, J. Kurkijärvi, M. Bauer, and W. Martienssen, in *Nonlinear Dynamics in Solids*, edited by H. Thomas (Springer-Verlag, Berlin, 1992).
- [12] J.-P. Eckmann, Rev. Mod. Phys. **53**, 643 (1981).
- [13] A. H. MacDonald and M. Plischke, Phys. Rev. B **27**, 201 (1983).
- [14] J. W. Swift and K. Wiesenfeld, Phys. Rev. Lett. **52**, 705 (1984).
- [15] W. C. Kerr, M. B. Williams, A. R. Bishop, K. Feser, P. S. Lomdahl, and S. E. Trullinger, Z. Phys. B **59**, 103 (1985).
- [16] J. Miles, Physica D **31**, 252 (1988).
- [17] N. Takimoto and M. Tange, Prog. Theor. Phys. **90**, 817 (1993).
- [18] M. Levi, Phys. Rev. A **37**, 927 (1988).
- [19] T. H. Yang, C. S. Wang, J. C. Huang, and Y. S. Gou, Phys. Rev. E **51**, 5279 (1995).
- [20] M. Octavio, Phys. Rev. B **29**, 1231 (1984).
- [21] A. A. Ignatov, K. F. Renk, and E. P. Dodin, Phys. Rev. Lett. **70**, 1996 (1993).
- [22] D. H. Dunlap, V. Kovanis, R. V. Duncan, and J. Simmons, Phys. Rev. B **48**, 7975 (1993).
- [23] A. A. Ignatov, E. Schomburg, J. Grenzer, K. F. Renk, and E. P. Dodin, Z. Phys. B **98**, 187 (1995).
- [24] K. N. Alekseev, G. P. Berman, D. K. Campbell, E. H. Cannon, and M. C. Cargo, Phys. Rev. B **54**, 10625 (1996).
- [25] K. N. Alekseev, E. H. Cannon, J. C. McKinney, F. V. Kusmartsev, and D. K. Campbell, Phys. Rev. Lett. **80**, 2669 (1998).
- [26] E. H. Cannon, F. V. Kusmartsev, and D. K. Campbell, Europhys. Lett. **56**, 842 (2001).
- [27] K. N. Alekseev and F. V. Kusmartsev, Phys. Lett. A **305**, 281 (2002).
- [28] K. Unterrainer, B. J. Keay, M. C. Wanke, and S. J. Allen, Phys. Rev. Lett. **76**, 2973 (1996).
- [29] S. Winnerl, E. Schomburg, J. Grenzer, H.-J. Regl, A. A. Ignatov, A. D. Semenov, K. F. Renk, D. G. Pavel’ev, Y. Koschurinov, B. Y. Melzer, et al., Phys. Rev. B **56**, 10303 (1997).
- [30] K. N. Alekseev, P. Pietiläinen, A. A. Zharov, and F. V. Kusmartsev (2001), to be published, arXiv:cond-mat/0111454.
- [31] N. F. Pedersen, O. H. Soerensen, B. Dueholm, and J. Mygind, J. Low Temp. Phys. **38**, 1 (1980).
- [32] A. P. Tetervov, Izv. VUZ Radiofiz. **27**, 801 (1984), [Engl. transl.: Radiophysics and Quantum Electronics (Consultant Bureau, New York) **27**, 564 (1984)].
- [33] F. G. Bass and A. P. Tetervov, Phys. Rep. **140**, 237 (1986).
- [34] K. N. Alekseev and A. Malkin (2004), unpublished.
- [35] S. Bumyalene, G. Lasene, and K. Piragas, Fiz. Tekhn. Polupr. **23**, 1479 (1989), [Sov. Phys. Semicond. **23**, 918 (1989)].
- [36] M. Abramowitz and I. Stegun, eds., *Handbook of Mathematical Functions* (Dover, New York, 1965), chap. 20.
- [37] J. R. Cash and A. H. Karp, ACM Trans. Math. Softw. **16**, 201 (1990).
- [38] J. R. Dormand and P. J. Prince, J. Comput. Appl. Math. **7**, 67 (1981).
- [39] G. Benettin, L. Galgani, A. Giorgilli, and J.-M. Strelcyn, Meccanica **15**, 9 (1980).
- [40] I. Shimada and T. Nagashima, Prog. Theor. Phys. **61**, 1605 (1979).
- [41] The pattern of symmetric inverted oscillations plus the nearest symmetry breaking region in our computations is found to be quite similar to the pattern described as “symmetry broken” for overdamped pendulum in ref.[13]. This might be explained observing that technique used in [13] to detect symmetry broken trajectories at strong damping can not in fact distinguish symmetric inverted and instant asymmetric solutions.